Flow and mixing characteristics of gas-liquid slug flow in a continuous Taylor-Couette flow reactor with narrow gap width

Shimizu, Keigo
Kato, Kairi
Kobayashi, Tomoyuki
Komoda, Yoshiyuki
Ohmura, Naoto

(Citation)
Chemical Engineering and Processing - Process Intensification,183:109226

(Issue Date)
2023-01

(Resource Type)
journal article

(Version)
Version of Record

(URL)
https://hdl.handle.net/20.500.14094/0100479013

Chemical Engineering & Processing: Process Intensification 183 (2023) 109226

Contents lists available at ScienceDirect

Chemical Engineering and Processing - Process Intensification

journal homepage: www.elsevier.com/locate/cep

Flow and mixing characteristics of gas-liquid slug flow in a continuous Taylor-Couette flow reactor with narrow gap width

Keigo Shimizu [a], Kairi Kato [b], Tomoyuki Kobayashi [b], Yoshiyuki Komoda [a], Naoto Ohmura [a,*]

[a] Department of Chemical Science and Engineering Graduate School of Engineering, Kobe University 1-1 Rokkodaicho, Nada-ku, Kobe, Hyogo, 657-8501, Japan
[b] Tipton Corp. 3-19-21 Toyoda, Minami-ku, Nagoya, 457-8566, Japan

ARTICLE INFO

Keywords:
Taylor-Couette flow
Gas-liquid two-phase flow
Hydrodynamics
Gas-liquid slug flow
Plug flow reactors

ABSTRACT

This work experimentally investigated flow characteristics and mixing properties of the two-phase flow in a continuous Taylor-Couette flow reactor (CTCR) with narrow gap width. In the device with a gap width of 0.5 mm, to the authors' knowledge, the narrowest gap width device ever studied in CTCR systems, the present study revealed that slug flows with alternating gas and liquid phases, as observed in microchannels, appeared in a certain flow regime. This slug flow appeared mainly in the region of low rotational Reynolds and axial Weber numbers. The non-dimensional effective diffusion coefficient D_{eff}/uL [-] of slug flow was also measured by a tracer response method. D_{eff}/uL in the slug flow was on the order of 10^{-6} and it has been successfully found that ideal plug flow mixing characteristics could be achieved under this flow condition. Since the intensified and controllable mixing in the liquid phase due to Taylor vortex motion induced by the inner cylinder rotation is expected to be much better than the mixing in the liquid phase of slug flows in microchannels, this flow is expected to be one of the process intensification techniques that will outperform the performance of the conventional microreactors with microchannels.

1. Introduction

Much attention has been paid to the conversion from batch to continuous process as one of the process intensification techniques that can dramatically improve process performance. In the pharmaceutical and fine chemical industries in particular, there are high expectations for continuous processes not only from the perspectives of energy and resource conservation and intrinsic process safety, but also as a means to produce highly functional substances with high precision. Static mixers [1], oscillatory baffled reactors (OBR) [2,3], and micro-reactors [4,5] have been developed for process intensification in these industries. A continuous Taylor-Couette reactor (CTCR) is also expected to be a potential continuous reactor to be applied to crystallization [6], homogeneous catalyzed reaction [7], polymerization [8], and particle classification [9], etc.

Taylor-Couette flow (TCF) is a typical sheared flow in the gap between two rotating coaxial cylinders and shows rich transitional phenomena from laminar to turbulent flow. It has been, therefore, investigated from the aspects of hydrodynamic stabilities, nonlinear dynamics and pattern formation for many years [10,11]. In most applications of TCF to chemical processes, the outer cylinder is kept stationary and only the inner cylinder is rotated. The fundamental dynamical parameter for TCF is the rotational Reynolds number $Re_\theta = \rho d R_i \omega/\mu$. In the low Re_θ region, laminar Couette flow which is purely circumferential flow is generated, and it transitions to laminar Taylor vortex flow (LTVF) when Re_θ exceeds a certain critical value. As shown in Fig. 1, LTVF consists of pairs of counter-rotating toroidal vortices spaced regularly along the cylinder axis. As further increases Re_θ, the sequential transitions of flow occur in the following order: wavy vortex flow, modulated wavy vortex flow, weakly turbulent (chaotic) vortex flow, turbulent vortex flow and finally turbulent flow without vortices. The inflow cell boundaries where flow is directed toward the inner cylinder present a barrier to intercellular mass transfer between two vortices as distinct from the outflow cell boundaries. A pair of vortices separated by two inflow boundaries can be, therefore, regarded as a well-mixed and independent mixing unit. It is also known that the vortex cells move in the axial direction in a single file while maintaining their shapes when the moderate rate of axial flow (low axial Reynolds number $Re_z = \rho d u_z/\mu$) is added. Kataoka et al. [12] focused on the flow and mixing characteristics of this LTVF and they first proposed that this flow could be applied as an ideal plug flow reactor. In addition, the large specific surface area and the impinging flow at each vortex boundary enhance the heat transfer on the cylinder walls, resulting in a very high

* Corresponding author.
E-mail addresses: 213t430t@stu.kobe-u.ac.jp (K. Shimizu), ohmura@kobe-u.ac.jp (N. Ohmura).

https://doi.org/10.1016/j.cep.2022.109226
Received 4 September 2022; Received in revised form 19 November 2022; Accepted 26 November 2022
Available online 28 November 2022

Nomenclature

$C(t)$	Tracer concentration at the outlet at time t [mol/m^3]
d	Gap width [m]
D_{eff}	Effective diffusion coefficient [m^2/s]
D_{eff}/uL	Vessel Peclet number [-]
D_{mol}	Molecular diffusion coefficient [m^2/s]
$E(t)$	E-function, RTDF
J	Mole flux [mol/s·m^2]
l	The axial length of the transparent part of the cylinder [mm]
L	The axial length of the region of interest [m]
L_{eff}	The effective axial length of the cylinder [m]
N	Rotational number [rpm]
$P(t)$	Normalized tracer concentration [-]
Q	Volumetric flow rate [m^3/s]
Q_{G}	The volume flow rate of gas [m^3/s]
Q_{L}	The volume flow rate of liquid [m^3/s]
$Q_{\mathrm{t}} = Q_{\mathrm{L}} + Q_{\mathrm{G}}$	The total gas-liquid flow rate [m^3/s]
R_{i}	The radius of the inner cylinder [m]
R_{o}	The radius of the outer cylinder [m]
Re_{c}	Critical Reynolds number of the system with $d = 0.5$ mm [-]
Re_{s}	Normalized Reynolds number [-]
Re_{z}	Axial Reynolds number [-]
Re_{θ}	Rotational Reynolds number [-]
t	Time [s]
u	Superficial velocity [m/s]
v_{G}	The superficial velocity of gas [m/s]
v_{L}	The superficial velocity of liquid [m/s]
u_{z}	Representative axial velocity [m/s]
We_{z}	Axial Weber number [-]
We_{θ}	Rotational Weber number [-]
z	Axial coordinate in CTCR [mm]

Greek letters

$\beta = Q_{\mathrm{L}}/Q_{\mathrm{G}}$	Flow ratio of liquid to gas [-]
δ	Vortex drift length [mm]
ε	Ratio of centrifugal force to buoyancy force [-]
$\eta = R_{\mathrm{i}}/R_{\mathrm{o}}$	radius ratio [-]
μ	Viscosity [Pa·s]
ρ	Density of liquid [kg/m^3]
ρ_G	Density of gas [kg/m^3]
σ (no index)	The surface tension of liquid [N/m]
σ (with index)	Variance of RTD function [s^2]
τ	Residence time [s]
φ_{i}	Inlet diameter [mm]
φ_{o}	Outlet diameter [mm]
ω	Angular velocity of the inner cylinder [rad/s]

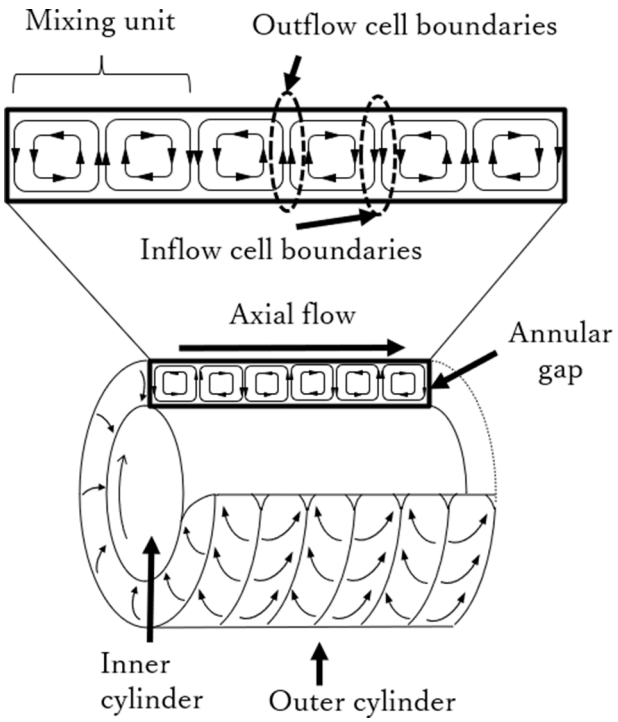

Fig. 1. Structure of Taylor vortex flow.

thermal response, which is very advantageous in crystallization reactions where temperature control is important, and in polymerization reactions where cooling is required for safety reasons.

Nguyen et al. [6] and Lee et al. [13] investigated the application of Taylor vortex flow (TVF) to crystallizer and reported the following advantages over conventional stirred tank reactors: shorter achieving time to a steady-state, the narrower size distribution of crystals, and better shape control of crystals due to the uniformity of TVF flow. Many studies investigate polymerization reactions in CTCRs. Wolinski and Wroński [14] claimed that the large specific surface areas are expected to enhance heat transfer in polymerization requiring cooling and that the residence time can be shortened compared to a stirred tank reactor. Liu et al. [8], and Kataoka et al. [15] found that controllable flow conditions provide a narrow particle size distribution and that particle coagulation can be prevented by the uniform shear forces each other. Applications to enzymatic transformations and biotechnology have also been investigated. It has been reported that the uniform and low shear field of TVF, where efficient mixing conditions can be obtained without damaging the contents, is advantageous in isomerization reactions using fragile materials such as immobilized enzymes [16]. Also, due to the improved aeration and controllability of shear stress, it is expected to be applied to the culture and manipulation of cells. Haut et al. [17] investigated the cultivation of animal cells in suspension both experimentally and numerically using PIV and CFD and found that the growth of cells depended on the average shear stress in the reactor. Other applications as a particle classifier have also been investigated by Ohmura et al. [9] and Kim et al. [18]. Small particles are trapped in the vortex core region and move slowly in the axial direction, while large particles move quickly in the axial direction due to the bypass flow outside the vortex, thus allowing the classification of particles according to size.

While TCFs have been applied in such a wide range of fields, the slug flow in a microchannel as a plug flow reactor has also been attracting attention. When gas and liquid phases are continuously supplied into a microchannel, various flow patterns such as annular, bubbly, dispersed, and slug flows are generated depending on the channel diameter, fluid flow rate, gas-liquid flow ratio, and fluid properties [19]. Among these flow patterns, the slug flow refers to the state in which fluid mass of each phase with a cross-sectional shape and area approximately equal to that of the channel flow in alternating lines. Depending on the wettability of the liquid phase and the channel wall, a liquid film may be formed on the channel wall. From a chemical engineering point of view, the slug flow in microchannels has many advantages such as narrow residence time distribution [20] and the large specific area for heat transfer and gas-liquid mass transfer [21], and has been applied to many chemical

Table 1
Previous studies deal with CTCR with narrow gap width [32–36].

d [mm]	R_i [mm]	R_o [mm]	Vertical or Horizontal	Authors	Year
1	12.5	13.5	Vertical	S. J. Curran et al.	2005
1	2.5~22	3.5~23	Vertical	C. Schäfer et al.	2018
2.5	27.5	30	Horizontal	R. Hubacz	2015
3	100	103	Horizontal	J. G. Lim et al.	2021
2.5	27.5	30	Horizontal	R. Hubacz et al.	2004

processes such as crystallization and gas-liquid two-phase reactions [20, 21]. On the other hand, it should be noted that the microchannels have some disadvantages such as easy clogging [22,23] and large pressure drop. About the pressure drop, many researchers have attempted to reduce the drag force inside the channel by adding polymers [24], changing the shape of the junction [25], or injecting gasses [26].

Various studies [27–29] have been conducted on the conditions for the occurrence of the slug flow, and these researches revealed that the slug flow occurs when the interfacial tension in the two-phase flow is sufficiently larger than the inertia force. For example, Yang and Shieh [30] reported, based on experimental data, that the slug flow was formed when the Weber number is less than 0.01.

The representative studies on gas-liquid two-phase flow behavior in CTCR are these by Shiomi et al. [31] and Hubacz et al. [32,33]. The flow regimes could be classified by using the relationship between power consumption and liquid mass flux [32], or by using Archimedes number [33], which is the ratio of buoyancy and viscous force. Their study observed various flow regimes such as stratified, periodic, disturbed slug, bubbly, and spiral flows. Although some of them are classified as slug flows, they should be distinguished from the slug flow which is observed in a microchannels because they do not fit the above characteristics of the slug flow in a micro-channel, which has a cross-sectional shape almost equal to the channel cross-section. Thinking in the same way as the case of the microchannel, when the gap width is narrow in CTCR, surface tension becomes dominant in the gas-liquid flow, and the slug flow can occur. In addition, the narrower gap width, the lower Re_θ at the same rotation, Taylor vortex cells are more stable while maintaining a good mixing in a unit of vortex cells. The authors believe that this paper is original in that it is the first observation of a slug-Taylor vortex flow with ideal plug flow-like characteristics. The previous studies on CTCR, focusing on the gap width, can be summarized as shown in Table 1. Among these previous studies, the gap width $d = 0.5$ mm and the radius ratio $\gamma = 0.98$ in this study are the narrowest width and the largest radius ratio. There are two types of CTCRs, i.e. vertical and horizontal. In the horizontal type, the axial movement of the gas phase due to the effect of buoyancy forces can be neglected, so the horizontal type was adopted in this study.

At first, this study investigated the single-phase flow behavior in CTCR with narrow gap width by visualization using aluminum platelet powder. Second the gas-liquid two-phase flow behaviors were experimentally investigated to classify the flow regimes. Finally, tracer response experiments were conducted to compare effective diffusion coefficients for single-phase and two-phase flows and to evaluate the

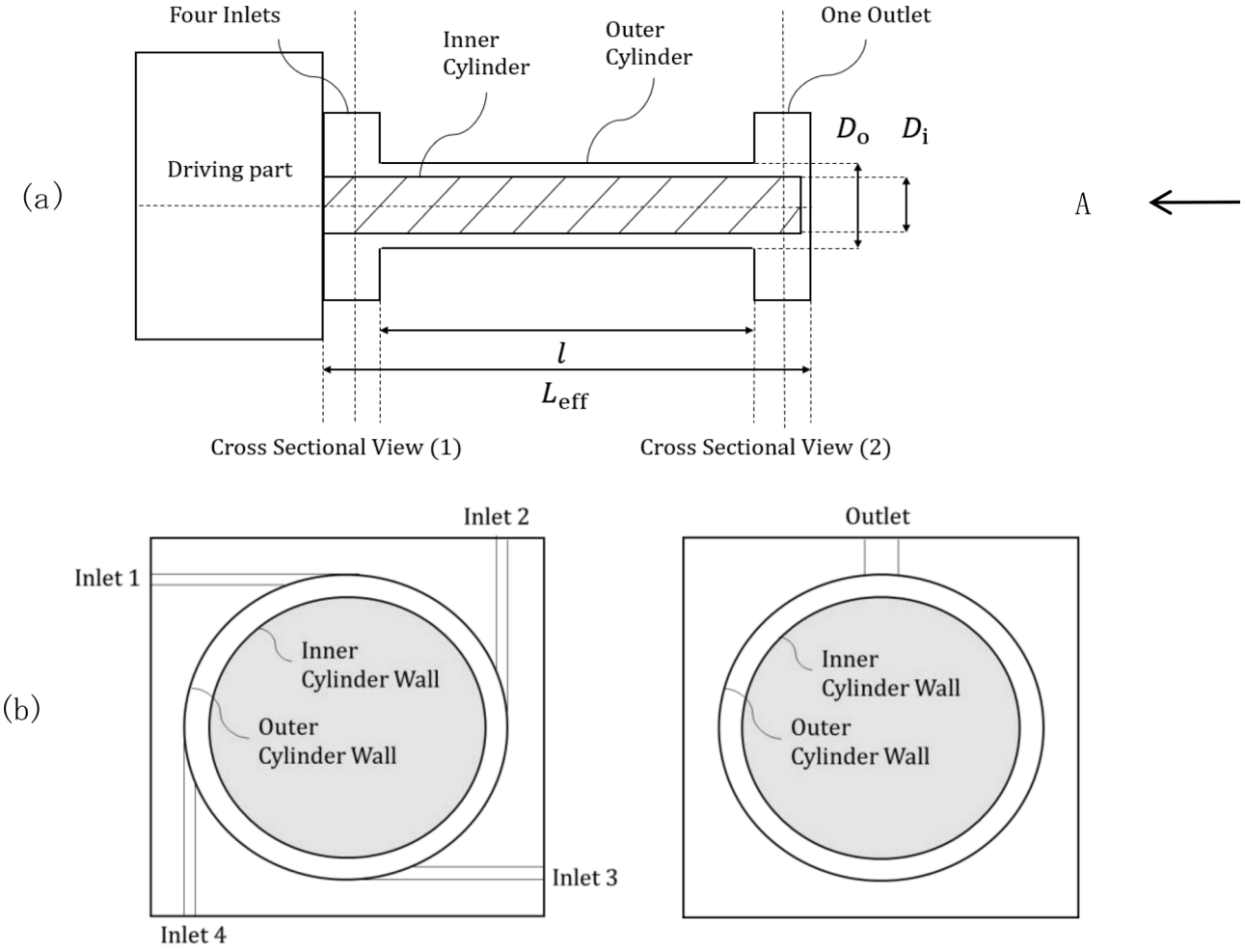

Fig. 2. Geometry of the CTCR., (b) shows the axial cross-sectional view, with cross sectional view (1) on the left and cross-sectional view (2) on the right. Each cross-sectional view is viewed from the direction of A.

mixing performance.

2. Experimental

2.1. Experimental apparatus

Concentric two cylinders with the inner cylinder rotating and the outer one at rest were installed horizontally as shown in Fig. 2. The outer cylinder with the inner diameter of $D_o = 50$ mm in the test section is made of transparent polycarbonate resin so that the flow in the gap can be visually observed. Three kinds of inner cylinders with different outer diameters of 49, 47.5 and 45 mm were used so that the gap width, d, varied 0.5, 1.25, and 2.5 mm, respectively. The effective axial length L_{eff} is 158 mm long, the length of the test section made of transparent cylinder is 106 mm ($= l$) long. The rotational speed of the inner cylinder can be set in the range of 0~3000 rpm. As shown in Fig. 2(b), the device has four inlets and one outlet, with the direction of flow at the inlets oriented tangential to the inner cylinder to avoid disturbing the formation of Taylor vortex cells. The inner diameters of the inlets and outlet are $\varphi_i =$ 3mm and $\varphi_o = 4$mm, respectively. Tap water was used as the working fluid, and the gas phase in the two-phase flow was air. The liquid and gas were supplied to the device using a tubing pump (FRONT LAB, 1–3490–01 FP300–1515).

2.2. Visualization of Taylor-Couette flow

A small amount (less than 0.05 vol.%) of thin aluminum flake-shaped powder (Fujifilm Wako Pure Chemicals Co., Ltd.) with 20 μm long side was added to the working fluid and used to visualize the Taylor vortex flow. Since the platelets are aligned along streamlines, the fluid appears light silverly where the fluid is moving parallel to an observer [37].

2.3. Operational conditions in CTCR

The stability of gas-liquid slug flow is affected by various operational parameters such as gas, liquid flow rate, gas-liquid flow ratio, liquid properties, channel diameter (in this case, the gap width), and channel geometry. In addition to these parameters, the effect of rotational speed of the inner cylinder on the gas-liquid two-phase flow behavior in the CTCR must be also taken into account. For simplification, this study investigated the effect of rotational speed of the inner cylinder, total gas-liquid flow rate, and gap width on the gas-liquid slug flow behavior and fixed the gas-liquid flow ratio β as unity. The gap width d, the total gas-liquid flow rate Q, and rotational speed (or rotation number N) of the inner cylinder were varied in the range of 0.5, 1.25, 2.5 mm, 5 to 120 mL/min, and 0 to 3000 rpm, respectively. The working fluid and air were supplied to the device using Inlets 1 and 4 in Fig. 2(b), respectively.

2.4. Tracer response experiments

To investigate the mixing characteristics of the gas-liquid slug flow in the CTCR, the effective diffusion coefficient of the reactor was measured by a tracer response method and compared between the single-phase and the two-phase flow. Iodine-starch solution was used as a tracer, and the time variation of concentration of iodine-starch complex was measured by taking the images in the gap area with a video camera (Panasonic DMC-GF7, frame rate: 25 fps, 480 × 272 pixels, pixel aspect ratio: 1, image scale: 0.275 mm/pixel) and measuring the change in brightness of the liquid phase by an image processing software, ImageJ (ver.1.8.0). Iodine-starch solution was used merely as a tracer dye without any chemical reactions. The original iodine-starch solution was prepared by adding 0.1 g of soluble starch (Nacalai Tesque, INC.) and 2.5 mL of iodine solution (FUJIFILM Wako Pure Chemical Corporation) to 100 mL of water. The dimensionless concentration of the iodine-starch complex is defined as the ratio of the concentration of each solution to that of the original solution. Iodine-starch solutions with

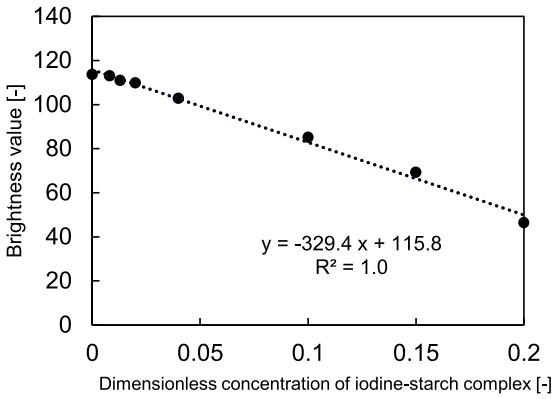

Fig. 3. Calibration line of solution of iodine-starch complex., Dimensionless concentration of iodine-starch complex is the ratio of the concentration of each solution to the concentration of the original solution.

dimensionless concentrations of 0~0.2 were prepared. The relationship between concentration and brightness values was investigated by filling the inside of the device with iodine-starch solution varying concentrations from 0~0.2 and taking pictures from the outside of the device. As a linear relationship was obtained between the dimensionless concentration and the brightness value (Fig. 3), the tracer concentration was obtained by converting the brightness value to the dimensionless concentration. Based on these considerations, a 1 mL tracer was impulsively injected by a syringe just before the liquid phase inlet (Inlet 1 in Fig. 2(b)) so that the dimensionless concentration could vary from 0 to 0.2 (Vessel volume is about 11 mL). Two measuring points were located with a certain distance in the axial direction and the effective diffusion coefficient was calculated by the following analysis method.

The impulse response method was used to quantify the degree of axial mixing diffusion based on the dispersion model. The residence time distribution function (RTDF), $E(t)$ is obtained by the tracer response experiments. RTDF can be calculated by introducing the tracer to the CTCR and measuring the change in the tracer concentration, $C(t)$, at the outlet of the vessel. $C(t)$ is normalized in the following manner as shown in Eq. (1), to obtain the normalized tracer concentration $P(t)$.

$$P(t) = \frac{C(t)}{\int_0^\infty C(t)\mathrm{d}t} \tag{1}$$

The amount of tracer discharged from the device between time t and $t + \mathrm{d}t$ can be expressed as $QC(t)\mathrm{d}t$, where Q is the volumetric flow rate. Dividing $QC(t)\mathrm{d}t$ by the total amount of tracer, the fraction of elements whose residence time is between t and $t + \mathrm{d}t$, i.e., $E(t)\mathrm{d}t$ is obtained.

$$\frac{QC(t)\mathrm{d}t}{\int_0^\infty QC(t)\mathrm{d}t} = E(t)\mathrm{d}t \tag{2}$$

For the impulsive tracer response, $E(t)$ theoretically corresponds to $P(t)$.

$$E(t) = \frac{C(t)}{\int_0^\infty C(t)\mathrm{d}t} = P(t) \tag{3}$$

For the diffusion of a substance in a reactor, not only the molecular diffusion but also the effect of fluid mixing due to convective flow motion must be taken into account. In general, the molecular diffusion coefficient D_{mol} [m^2/s] of a substance is on the order of 10^{-10}, but the effective diffusion coefficient D_{eff}/uL [-] considering fluid mixing is on the order of 10^{-2}~10^{-1}. Therefore, it is important to evaluate the effective diffusion coefficient to understand the mixing characteristics in the reactor. D_{eff}/uL [-] (vessel dispersion number or vessel Peclet number) is often used as a dimensionless number to characterize the diffusion of the entire vessel. Here, L [m] is the axial length of the region of interest. If D_{eff}/uL is close to zero, the flow in the device is close to a plug flow, and if D_{eff}/uL is close to infinity, the flow is close to that of a

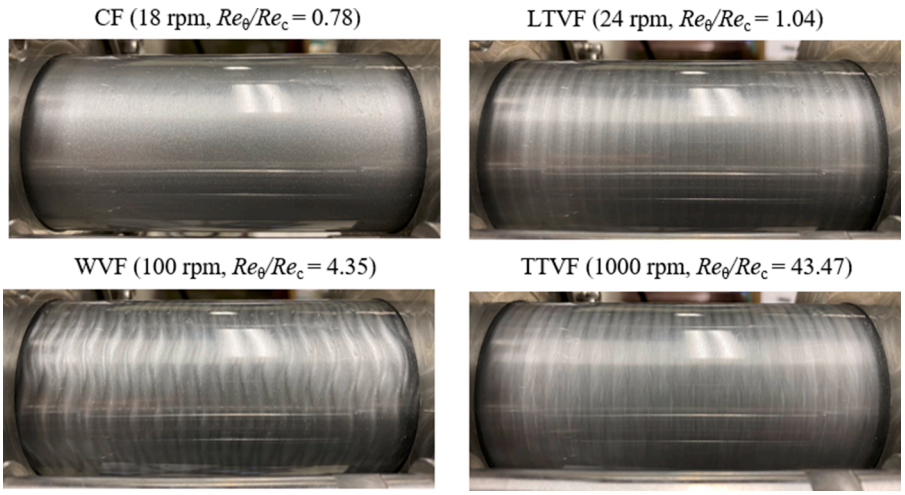

Fig. 4. Visualized Taylor-Couette flow of each flow regime., $d = 2.5$ mm, $Re_c = 135.5$, Working fluid is water (CF: Couette flow, LTVF: Laminar Taylor vortex flow, WVF: Wavy vortex flow, TTVF: Turbulent Taylor vortex flow).

CSTR. The one-dimensional mass transfer in the z-axis direction including the effect of fluid mixing is expressed by Eq. (4), where, C [mol /m^3] is the molar concentration of the tracer at the axial position z [m] and time t [s], and J [mol /(m^2·s)] is mole flux.

$$J = -D_{\text{eff}}\left(\frac{\partial C}{\partial z}\right) \tag{4}$$

In the dispersion model, mass transfer in a continuous tubular reactor is attributed to axial convection and one-dimensional dispersion only, and the radial direction is considered to be completely mixed without concentration distribution. Based on the dispersion model, the following partial differential equation is obtained by taking the mass balance in the axial direction (z-direction) and transforming it into a differential form,

$$\frac{\partial C}{\partial t} = D_{\text{eff}}\frac{\partial^2 C}{\partial z^2} - u\frac{\partial C}{\partial z} \tag{5}$$

where u [m /s] is the linear axial velocity.

To solve this partial differential equation, the initial and boundary conditions are necessary. Two types of boundary conditions which depend on the inlet and outlet conditions have been considered. The first is an ideal system called the closed vessel model, where the flow in the device is non-ideal, but the fluid at the inlet and outlet is in a plug flow condition, which is often assumed to facilitate theoretical analysis. The other system is called the open vessel model, which is a real system with the non-ideal flow at the inlet and outlet, like a section in a tubular reactor. In this study, the open vessel model is adopted. When the flow condition in the open vessel is close to a plug flow, the approximate solution of Eq. (5) for impulse input is given as follows.

$$C = \frac{1}{\sqrt{4\pi\frac{D_{\text{eff}}}{uL}}}\exp\left(-\frac{\left(1-\frac{t}{\tau}\right)^2}{4\frac{D_{\text{eff}}}{uL}}\right) \tag{6}$$

where τ [s] is the mean residence time based on volume flow rate. Converting this to the RTDF, the following Eq. (7) is obtained.

$$E(t) = \sqrt{\frac{u^3}{4\pi D_{\text{eff}}L}}\exp\left(-\frac{(L-ut)^2}{\frac{4D_{\text{eff}}L}{u}}\right) \tag{7}$$

The mean residence time t_{ave} [s] obtained by Eq. (8) and the variance σ_0^2 [s^2] obtained by Eq. (9) are theoretically related to D_{eff}/uL, and D_{eff}/uL can be calculated by Eq. (10) [38].

$$t_{ave} = \int_0^\infty tE(t)dt \tag{8}$$

$$\sigma_0^2 = \int_0^\infty (t - t_{\text{ave}})^2 E(t)\mathrm{d}t \tag{9}$$

$$\frac{D_{\text{eff}}}{uL} = \frac{1}{2}\left(\frac{\sigma_0^2}{t_{\text{ave}}^2}\right) \tag{10}$$

However, since this is a solution for an ideal impulse input, it is not suitable for analysis of real systems. Therefore, an estimating equation corresponding to Eq. (10) has been derived for non-ideal inputs by Aris [39]. Aris reported that D_{eff}/uL can be calculated as follows

$$\frac{D_{\text{eff}}}{uL} = \frac{1}{2}\left(\frac{\Delta\sigma_0^2}{(\Delta t_{\text{ave}})^2}\right) = \frac{1}{2}\frac{\sigma_{\text{in}}^2 - \sigma_{\text{out}}^2}{(t_{\text{ave. in}} - t_{\text{ave. out}})^2} \tag{11}$$

Each symbol means ave.: averaged, out and in: at the outlet and at the outlet, respectively. For example, $t_{\text{ave.in}}$ is the averaged residence time of the tracer at measuring point near the inlet. In this equation, Levenspiel [38] claimed that the error is less than 5% when $D_{\text{eff}}/uL < 0.01$. In this study, the RTDF was calculated from the changes of brightness in time at two points along the CTCR axis and D_{eff}/uL was estimated by Eq. (11) to evaluate the mixing characteristics.

3. Results and discussions

3.1. Flow visualization

The approximate critical Reynolds number was confirmed by visualizing the transition of the Taylor vortex in a device with 2.5 mm gap width using thin aluminum flake-shaped powder. The visualized images at each Reynolds number are shown in Fig. 4. As a result, the critical Reynolds number Re_c where CF transitions to LTVF was determined to be about 135.5. In $d = 0.5$, 1.25 mm ($\eta = 0.98$, 0.95) systems, although visualization was possible, it was difficult to discriminate the flow regimes. This study, therefore, adopted the critical Reynolds number, $Re_c \approx 135.5$ as an approximation in all gap widths.

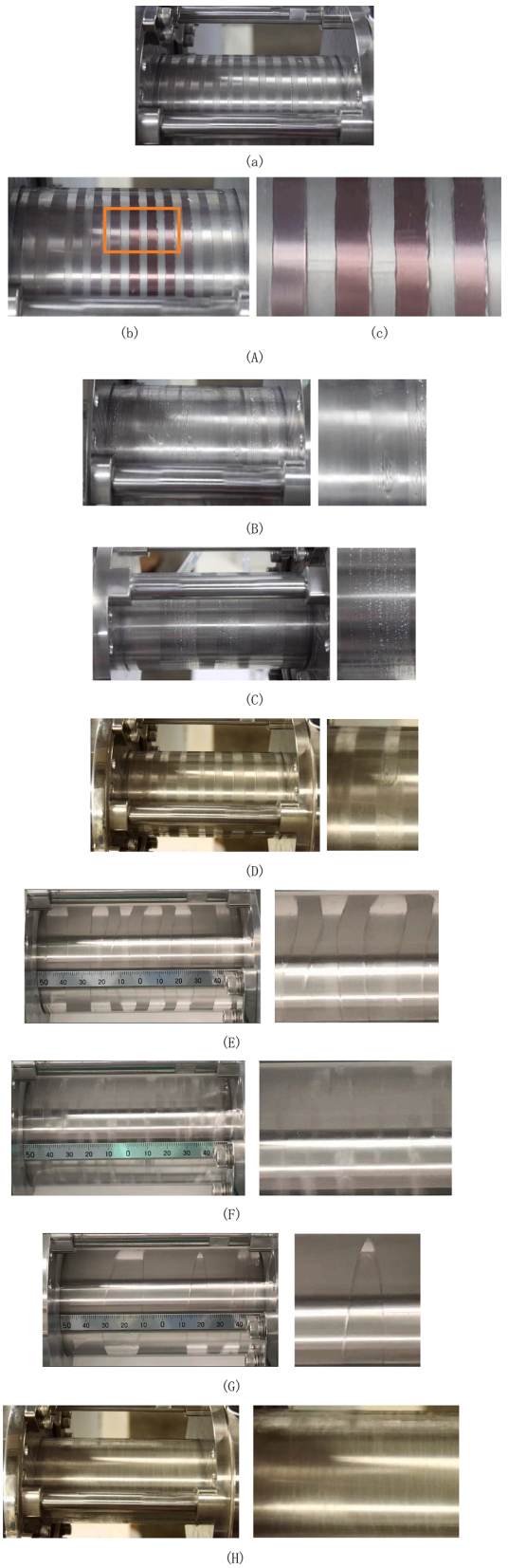

Fig. 5. Various gas-liquid flow regimes in CTCR Gap width: (A)~(E), (G), (H) d = 0.5 mm, (F) d = 2.5 mm., Flow conditions: Gas/liquid flow rate [mL/min], Rotation number [rpm] (A)15/15, 700 (B)15/120, 2000 (C)15/30, 2500 (D) 15/15, 2000 (E)15/15, 1000 (F)15/15, 1000 (G)150/90, 700 (H)15/15, 3000. *For B,C,G, gas-liquid flow ratio is not unity. Videos are available as supplement materials.

3.2. Gas-liquid flow regimes

Fig. 5 shows the photographs of the characteristic flow states observed in CTCR, along with the conditions under which they were observed. Fig. 5(A)-(a) is an ideal gas-liquid slug flow, in which the gas and liquid phases are almost equally spaced and the gas-liquid interface is stable. Another feature is that there is no liquid film between the liquid slugs, and this is confirmed by the following facts. Fig. 5(A)-(b) shows an ideal slug flow observed by a tracer response experiment. If liquid film layer exists in a gas phase, the purple color of the tracer should be seen between liquid slugs, but Fig. 5(A)-(c) which is the enlarged rectangular area surrounded by orange lines in Fig. 5(A)-(b) shows no purple color in the gas phase. It can be, therefore, considered that there is no liquid film layer in the gas phase. This slug flow was observed only in the system with the smallest gap width (d = 0.5 mm). Therefore, the narrow gap width plays an important role in the gas-liquid two-phase flow condition in CTCR. In the case of Fig. 5(B), a gas-liquid slug flow was locally going back and forth in between two adjacent liquid slugs in the axial direction while drifting in the axial direction, which also led to the coalescence of the liquid slugs (see Fig. 6). In the case of Fig. 5(C), liquid droplets were adhering to the cylindrical wall. These water droplets are considered to be generated by the separation of the liquid slug due to the shear force which the rotation of the inner cylinder caused during the axial movement. Fig. 5(D) is a gas-liquid slug flow with a liquid film. Features such as Fig. 5(B)~(D) can be seen under the same flow condition. In the case of Fig. 5(E), the gas-liquid interface of the gas-liquid slug flow is observed to be wavy. Since the wavy vortex flow is also observed in the transition phenomenon of the liquid single-phase Taylor-Couette flow system, it is assumed that the gas-liquid interface of the gas-liquid slug flow has similar characteristics to the vortex boundary of the TVF. Fig. 5 (F) shows bubbles moving in the circumferential direction in the continuous liquid phase. This is often seen in systems with larger gap widths (d = 1.25, 2.5 mm), and is similar to the fluid state that Shiomi et al. [31] reported. In the case of Fig. 5(G), the gas-liquid interface appears irregularly, and no clear gas or liquid slug can be seen. Fig. 5(H) is a state in which the gas-liquid interface is so disturbed that it cannot be determined at all.

The above eight flow states were classified into three in order of expected smaller mass transfer due to the axial mixing dispersion as follows.

Ideal slug flow: (A)
Non-ideal slug flow: (B)(C)(D)(E)
Disturbed flow: (F)(G)(H)

In the case of ideal slug flow, only the gas phase exists between the liquid-phase slugs, and there is no liquid-liquid contact or liquid-liquid exchange, so it is expected that there is almost no mass transfer between the liquid phases, i.e.; no axial dispersion. In the flows classified as ideal slug flows, a phenomenon has been observed sometimes in which the slug interface has wavy motions near the inlet of the equipment, and the wavy characteristics disappear near the center of the equipment (see Fig. 7). This phenomenon is caused by the frictional heat generated from the sliding parts near the inlet, which reduced the viscosity of the fluid and increased local Re_θ near the inlet. In the case of non-ideal slug flow, mass transfer is expected to occur through water droplets or liquid film, or coalescence of liquid phases due to the oscillatory or wavy motion of the interface. Disturbed flow is expected to have the same level of mass transfer as the single-phase Taylor-Couette flow system because the gas-liquid interface is unclear or liquid phase is continuous in the whole range of axial direction.

3.3. Mapping of flow states

Here, two parameters were used to produce a flow pattern map of the slug flow. The first is the rotational Reynolds number Re_θ as a parameter of rotation. The rotational Reynolds number was used to consider the stability of the slug flow in relation to the stability of the Taylor-Couette

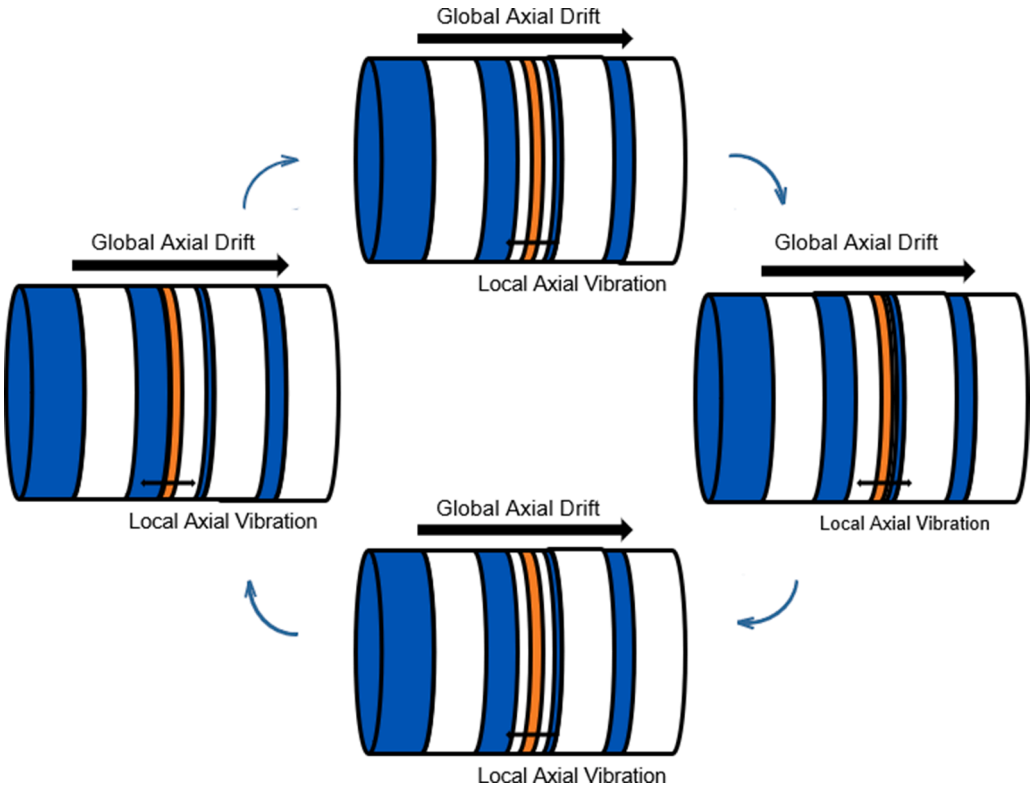

Fig. 6. Schematic diagram of vibrating liquid slug The liquid slug painted orange is locally going back and forth in between two adjacent liquid slugs in the axial direction. This diagram shows the change of the position of the liquid slug in a very short time. Blue or orange area: Liquid slugs, White area: Gas slugs.

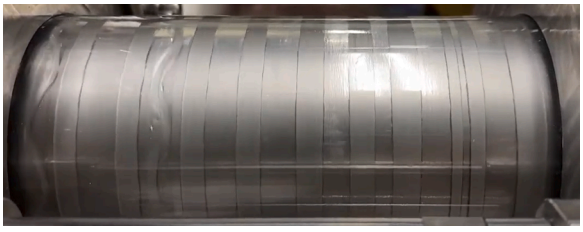

Fig. 7. Wavy motion near the inlet of the device.

flow. The second is the axial Weber number We_z, because the relationship between the interfacial tension and the inertia force is said to be important in the generation of slug flow in a typical circular tube [28]. Axial Weber number is defined as follows using total axial velocity. Fig. 8 shows the flow map of the gas-liquid slug for three kinds of gap width.

$$We_z = \frac{\rho d(v_L + v_G)^2}{\sigma} \tag{11}$$

Fig. 8 shows that ideal slug flow occurs only in the system with the minimum gap width of $d = 0.5$ mm. Flow regime distribution for the system with $d = 0.5$ mm is a little complicated. For industrial applications, it is desirable to know the maximum gap width to produce the ideal slug flow. It is, however, currently difficult to experimentally determine the maximum gap width where gas-liquid slug flow occurs because it requires the preparation of many cylinders. A CFD analysis will be conducted to confirm the maximum gap in our future work. The maximum gap width is also expected to vary depending on the physical properties of the liquid used. In fact, our experiments have already confirmed that in a system with $d = 1.25$ mm, slug flow occurs when an aqueous solution of glycerol is used.

In the system with $d = 1.25$ mm, only non-ideal slug flows and disturbed slug flows can be generated, and Re_θ region where non-ideal slug flows are generated is narrower than that of the system with $d = 0.5$ mm. With the gap width of $d = 2.5$ mm, no slug flow could be confirmed. This indicates that the narrow gap width is very important for the generation of gas-liquid slug flow in the CTCR.

In Fig. 8(a) and (b), the disturbed flows can be classified into two categories, buoyancy dominating flows and rotation dominating flows. Buoyancy dominating flows occur in low rotational speed region, lower gray dotted area in Fig. 8(a) and (b). On the other hands, rotation dominating flows occur in high rotational speed region, upper gray dotted area Fig. 8(a) and (b).

3.3.1. *The effect of rotational motion on stability of gas-liquid slug*

The change of the flow state with increasing rotation speed should be considered in relation with the transition phenomena of the Taylor-Couette flow. Fig. 9 is made based on Fig. 8 and shows the changes of flow regimes of TCF or slug state with the change of normalized Reynolds number Re_s.

Comparing the (i), (ii) and (iii), in the low Re_θ region, which is close to the Couette flow region, the buoyancy force is dominant, and the gas-liquid interphase is nearly horizontal. As the Re_θ increases to near Re_c, the gas-liquid slug flow stabilizes as the Taylor vortex boundary stabilizes. As the Re_θ increases and wavy Taylor vortex flow appears, the gas-liquid interface becomes unstable and liquid films and droplets are formed. Under some axial flow conditions, for example Fig. 9(ii), as Re_θ further increases, the slug stabilizes again. This phenomenon occurs when Re_s is around 24 and is caused by the stabilizing effect of the Taylor vortex boundary as the Taylor-Couette flow becomes TTVF, which also stabilizes the gas-liquid interface. Under the relatively high axial Weber number conditions ($We_z > 1.26 \times 10^{-4}$), for example Fig. 9 (iii), this phenomenon does not occur. At last, when Re_θ exceed a certain value, gas-liquid interface becomes indistinguishable because of the turbulence of Taylor vortex flow.

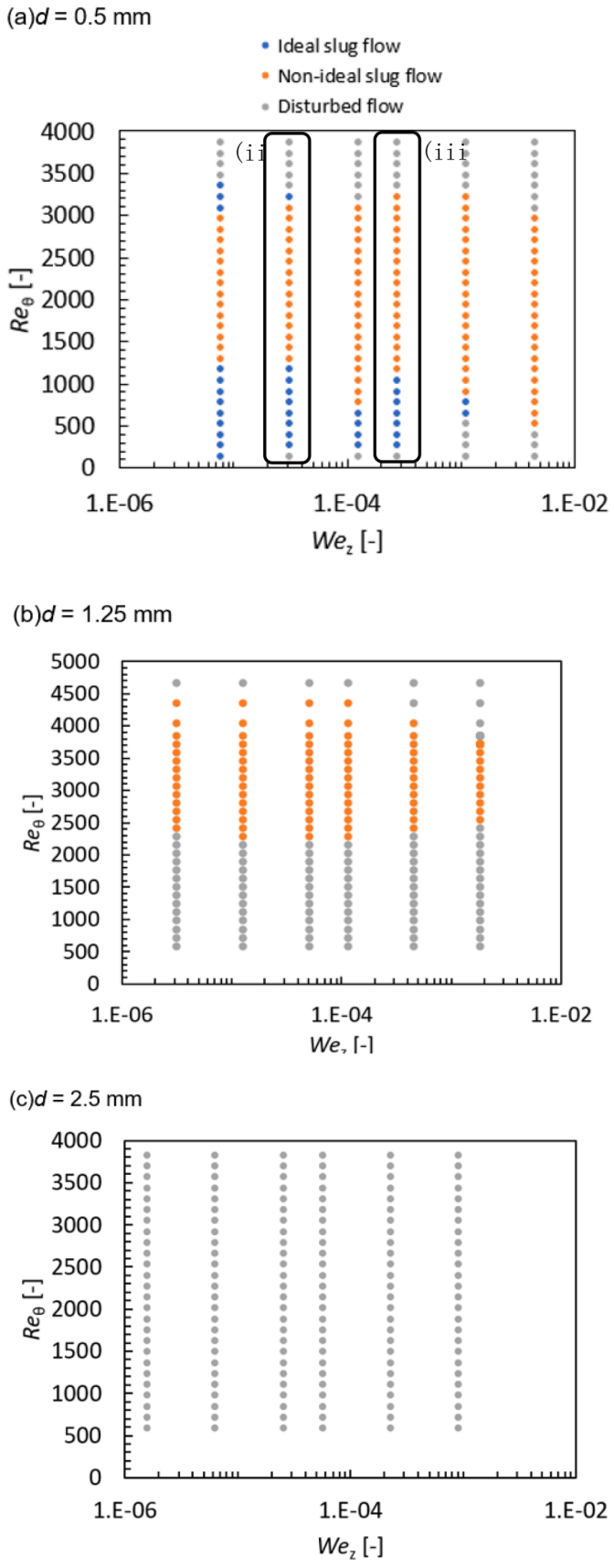

Fig. 8. Flow map of gas -liquid two phase flow in CTCR Enclosed area in (a) corresponds to Fig. 9. (ii)(iii).

3.3.2. *The effect of axial flow on stability of gas-liquid slug*

The effect of axial flow on slug stability can be considered in the same way as the stability of gas-liquid slug flow in a straight pipe; Dessimoz et al. [28] claimed that when the inertial force is larger than the surface tension, the shape of the bubble forming the slug is deformed from a sphere to a flat shape, causing the slug flow to transition to an annular slug flow. In the case of gas-liquid slug flow in the CTCR, the bigger the We_z, the narrower the rotation speed region where the ideal slug flow is stable, and the inertial force tends to cause deformation of the gas-liquid interface shape, which destabilizes the slug.

Seeing Fig. 8, even in the same (Re_θ, We_z) range, different gap widths will result in different flow conditions. This indicates that not only these dimensionless numbers of flow, but also dimensionless numbers of liquid properties and device geometry must be taken into account in the future work.

3.3.3. *The effect of gap width*

The reason why the ideal slug flow occurs only when the gap width is narrow is discussed in this section. In Section 3.3, the effect of axial flow has been investigated using We_z. Since We_z based on the axial flow is too small to explain the effect of the gap width for all three kinds of gap width systems. On the other hand, since We_θ based on the rotational speed of the inner cylinder is the ratio of rotational inertia force (centrifugal force) to surface tension, the values of We_θ are enough large to explain the effect of the gap width. However, the discussion using We_θ is only valid under conditions where the effects of other forces on the system could be neglected. The experimental results showed that a buoyancy dominating flow condition existed under the low rotation number condition, as discussed in Section 3.3. Therefore, this study calculated the ratio of centrifugal force to buoyancy force, ε defined as follows in Eq. (12), and the discussion was conducted using We_θ under the condition that the buoyancy force was negligible. Since the present system is considered to have a narrow gap width and a large effect of curvature, We_θ is redefined as follows in Eq. (13) by taking the curvature into account similar to the definition of Taylor number including a correction term for the effect of curvature.

$$\varepsilon = \frac{\rho(R_i\omega)^2}{(\rho-\rho_G)gd} = \frac{(R_i\omega)^2}{\left(1-\frac{\rho_G}{\rho}\right)gd} \approx \frac{(R_i\omega)^2}{gd}\left(\because 1-\frac{\rho_G}{\rho}\approx 1\right) \tag{12}$$

$$We_\theta = \frac{\rho d(R_i\omega)}{\sigma}\left(\frac{d}{R_i}\right)^{0.5} \tag{13}$$

Then, this study calculated the rotation speed range in which the inertia force is considered sufficiently large compared to the buoyancy force at each gap width, i.e., $\varepsilon > 100$ (Table 2).

Under the rotational speed range in Table 2, We_θ is used to determine the critical value at which the ideal slug flow occurs. In the case of $d =$ 0.5 mm, an ideal slug flow is formed in the rotational speed range of 100~900 rpm. If the speed range where $\varepsilon > 100$ is taken into account, the speed range is about 300~900 rpm, which is $0.26 < We_\theta < 5.23$. This indicates that the ideal slug flow occurs when $We_\theta < 5.23$. We have confirmed that no ideal slug flow occurs in the system with $d = 1.25$ and 2.5 mm. When $\varepsilon > 100$ in the cases of $d = 1.25$ and 2.5 mm, We_θ is larger than 6.1 and 31, respectively, which are out of the We_θ range where the ideal slug flow occurred in the case of $d = 0.5$ mm. From the above discussion, it can be considered that the ideal slug flow can occur when $\varepsilon > 100$ and $We_\theta < 5.23$. However, for $d = 0.5$ mm, the ideal slug flow occurs in the higher rotational speed region. This requires further consideration because the Weber number exceeds 5.23.

3.3.4. *Comparison with conventional microreactors and slug flow reactors*

The CTCR in this study was compared with conventional microreactors with microchannels and gas-liquid slug flow reactors, respectively.

The flow rate in a typical microreactor with channel width of about

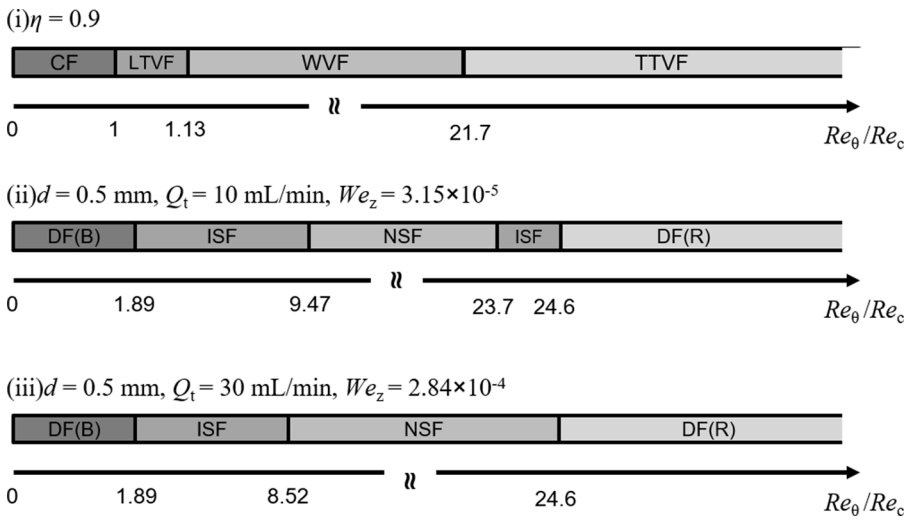

Fig. 9. Dependence of $Re_s(=Re_\theta/Re_c)$ on flow regimes (i) Single phase system without axial flow, (ii)(iii) Two phase flow systems, Re_c=135.5, η: Radius ratio [-], d: Gap width [mm], Q_t: Total flow rate [mL/min], We_z: Axial Weber number., (CF: Couette flow, LTVF: Laminar Taylor vortex flow, WVF: Wavy vortex flow, TTVF: Turbulent Taylor vortex flow, DF(B): Disturbed flow (buoyancy dominating), ISF: Ideal slug flow, NSF: Non-ideal slug flow, DF(R): Disturbed flow (rotation dominating))., (i) is made based on the visualization experiment in the chapter 2.2. (ii)(iii) corresponds to enclosed areas in Fig. 8(a).

Table 2
Rotation speed for $\varepsilon > 100$ at each gap width.

d [mm]	Rotation speed forε>100 [rpm]
0.5	275
1.25	450
2.5	675

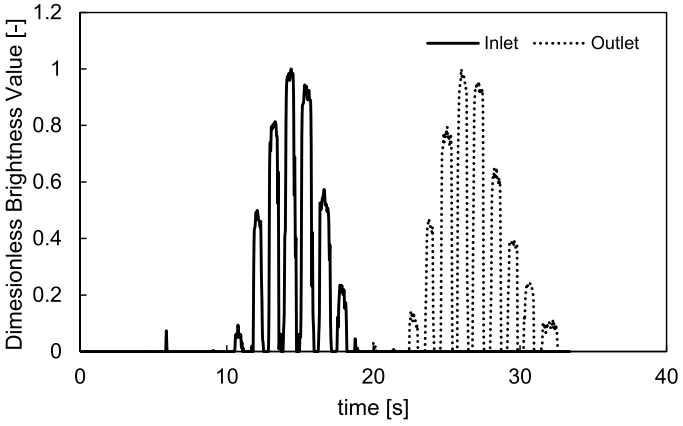

Fig. 10. Change of tracer concentration in time.

500 μm is about 0.02~1 mL/min [40–42], while the gas-liquid slug flow in this paper has a liquid phase flow rate of 5~30 mL/min. Thus, when compared with these two reactors from the aspect of volumetric flow rate, the production rate of the slug flow in the CTCR is superior in that it has a much larger production rate than the microfluidic reactors. This can eliminate the need for numbering up.

The mixing state inside the slug is considered to be determined by the internal circulation flow. In general gas-liquid slug flows in a microchannel, the circulation flow velocity is 20~300 mm/s [43]. On the other hand, the circulation velocity of a Taylor vortex is reported to be about 0.15 times the rotating velocity of the inner cylinder. Based on this calculation, the circulation velocity of the Taylor vortex in the liquid slug generated in the CTCR is estimated to be about 200~mm/s under the conditions in which the ideal slug flow is confirmed in this paper [44]. Therefore, the mixing in the slugs in the CTCR is expected to be very rapid compared to that in conventional slug flow reactors.

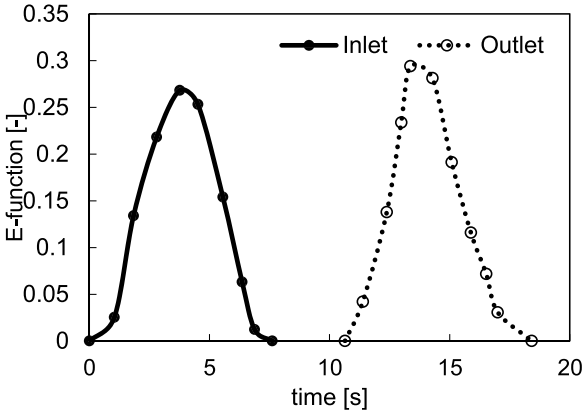

Fig. 11. Calculated RTDF.

Table 3
D_{eff}/uL for different flow conditions (d = 0.5 mm, τ = 24.6 s).

Flow pattern	Flow Condition	D_{eff}/uL [-]
Ideal slug flow	Q_L = 15 mL/min Q_G = 15 mL/min, N = 700 rpm	5.76 × 10^{-6}
Non-ideal slug flow	Q_L = 15 mL/min Q_G = 15 mL/min, N = 2000 rpm	3.91 × 10^{-3}
Single-phase Taylor-Couette flow	Q_L = 30 mL/min Q_G = 0 mL/min, N = 1500 rpm	1.50 × 10^{-2}

3.4. Mixing properties of slug flow in CTCR

The tracer response analysis was conducted for three flow states: Ideal slug flow, non-ideal slug flow, and single-phase system with the same residence time τ = 24.6s and gap width d = 0.5 mm. For the single-phase system, D_{eff}/uL was also calculated using the same method as introduced in Section 2.4. Fig. 10 shows the time variation of tracer concentration at the inlet and outlet of the test section in the ideal slug flow, where the concentration is nondimensionalized by the maximum concentration and is zero at the time when the gas phase or pure water passes through the position. The change has a peak corresponding to the liquid phase slug containing the tracer, and between the peaks, there is a time when the gas phase is passing through. By extracting the value of this peak and subtracting the time when the gas phase is passing

through, an RTDF eliminating gas phase effect was calculated (see Fig. 11). The values of D_{eff}/uL calculated by the analysis are shown in Table 3. In the ideal slug flow system, the value of D_{eff}/uL is on the order of 10^{-6}, which is very small compared to other conditions, and it can be said that there is almost no axial dispersion (The flow can be regarded as a plug flow when D_{eff}/uL is less than 0.01 [38]). In the single-phase system, there is some degree of mixing diffusion on the order of 10^{-2}. In non-ideal slug flow system, the order of D_{eff}/uL drops from the single-phase case, indicating that the axial dispersion is suppressed. Comparison with the case of the ideal slug flow also suggests that there is mass transfer some degree through liquid films and water droplets.

4. Conclusions

The behavior of gas-liquid two-phase flow in a CTCR with a narrow gap width was investigated, and it was found that an ideal gas-liquid slug flow with a cross-sectional shape almost equal to the channel cross-section was generated in a certain flow condition only in the narrowest annular gap system. The flow states of the gas-liquid slug flow in the CTCR were found to be considered in the relation with the stability of the Taylor vortex flow. When the effects of rotational and axial flows were organized by Re_θ and We_z, it was found that gas-liquid slug flow tended to occur when surface tension was dominant and reflected the stability of Taylor-Couette flow. On the other hand, different behaviors were observed at different gap widths even under the same (Re_θ, We_z) conditions. It is, therefore, necessary to find an evaluation variable that takes the effect of gap width into account in the future. The measured residence time distribution of the ideal gas-liquid slug flow showed that the effective diffusion coefficient was the order of 10^{-6} indicating the axial dispersion properties are almost the same as PFR. In addition, compared to microreactors, clogging may not occur in CTCR because the liquid is well-mixed by the rotation of the inner cylinder, and the pressure drop is also expected to be smaller. Another advantage is that the production speed can be much faster than that of microreactors. Therefore, the CTCR with a narrow gap using slug flow can be a new reactor system to replace conventional microreactors with microchannels.

CRediT authorship contribution statement

Keigo Shimizu: Data curation, Formal analysis, Methodology, Investigation, Writing – original draft. **Kairi Kato:** Conceptualization, Project administration, Resources. **Tomoyuki Kobayashi:** Conceptualization, Project administration, Resources. **Yoshiyuki Komoda:** Data curation, Validation. **Naoto Ohmura:** Conceptualization, Funding acquisition, Methodology, Project administration, Supervision, Writing – review & editing.

Declaration of Competing Interest

The authors declare that they have no known competing financial interests or personal relationships that could have appeared to influence the work reported in this paper.

Data availability

Data will be made available on request.

Acknowledgments

This research was supported by JSPS KAKENHI Grant Nos. JP18H03853 and JP 19KK0127.

Supplementary materials

Supplementary material associated with this article can be found, in the online version, at doi:10.1016/j.cep.2022.109226.

References

[1] K.M. Thomas, B.W. Nyande, R. Lakerveld, Design and characterization of Kenics static mixer crystallizers, Chem. Eng. Res. Des. 179 (2022) 549–563, https://doi.org/10.1016/j.cherd.2022.01.025.
[2] M.F.M.G. Resul, A. Rehman, A.M.L. Fernández, V.C. Eze, A.P. Harvey, Continuous process for the epoxidation of terpenes using mesoscale oscillatory baffled reactors, Chem. Eng. Process. - Process Intensif. 177 (2022), 108998, https://doi.org/10.1016/j.cep.2022.108998.
[3] M.S.R. Abbott, G. Valente Perez, A.P. Harvey, M.K. Theodorou, Reduced power consumption compared to a traditional stirred tank reactor (STR) for enzymatic saccharification of alpha-cellulose using oscillatory baffled reactor (OBR) technology, Chem. Eng. Res. Des. 92 (2014) 1969–1975, https://doi.org/10.1016/j.cherd.2014.01.020.
[4] X. Zhang, L. Zhong, G. Zeng, Y. Gu, C. Peng, F. Yu, Z. Tang, Y. Sun, Process intensification of honeycomb fractal micro-reactor for the direct production of lower olefins from syngas, Chem. Eng. J. 351 (2018) 12–21, https://doi.org/10.1016/j.cej.2018.06.078.
[5] S. Ouchi, H. Morikawa, M. Hara, T. Yamamoto, Nanosizing of polymeric particles by suppressing growth via heterocoagulation using a 3D micro-network reactor, Powder Technol. 405 (2022), 117530, https://doi.org/10.1016/j.powtec.2022.117530.
[6] A.T. Nguyen, T. Yu, W.S. Kim, Couette-Taylor crystallizer: effective control of crystal size distribution and recovery of L-lysine in cooling crystallization, J. Cryst. Growth. 469 (2017) 65–77, https://doi.org/10.1016/j.jcrysgro.2016.10.020.
[7] A. Behr, T. Färber, Application of a Taylor-Couette reactor in homogeneous catalysis, Chem. Eng. Trans. 43 (2015) 835–840, https://doi.org/10.3303/CET1543140.
[8] Z. Liu, T. Jin, M. Kind, Continuous polymerization of methyl methacrylate in a taylor-couette reactor. I. Influence of fluid dynamics on monomer conversion, Polym. Eng. Sci. (2013) 96–104, https://doi.org/10.1002/pen.23245.
[9] N. Ohmura, T. Suemasu, Y. Asamura, Particle classification in Taylor vortex flow with an axial flow, J. Phys. Conf. Ser. 14 (2005) 64–71, https://doi.org/10.1088/1742-6596/14/1/009.
[10] A. Mallock, Determination of the viscosity of water, Proceeding R. Soc. Lond. 45 (1889) 126–132, https://doi.org/10.1098/rspl.1888.0081.
[11] G.I. Taylor, stability of a viscous liquid contained between two rotating cylinders, Philos. Trans. R. Soc. 223 (1923) 289–343, https://doi.org/10.1098/rsta.1923.0008.
[12] K. Kataoka, H. Doi, T. Hongo, M. Futagawa, Ideal plug-flow properties of taylor vortex flow, J. Chem. Eng. Jpn. 8 (1975) 472–476, https://doi.org/10.1252/jcej.8.472.
[13] S. Lee, C.H. Lee, W.S. Kim, Taylor vortex effect on flocculation of hairy crystals of calcium lactate in anti-solvent crystallization, J. Cryst. Growth. 373 (2013) 32–37, https://doi.org/10.1016/j.jcrysgro.2012.10.012.
[14] J. Woliński, S. Wroński, Interfacial polycondensation of polyarylate in Taylor-Couette-Reactor, Chem. Eng. Process. Process Intensif. 48 (2009) 1061–1071, https://doi.org/10.1016/j.cep.2009.02.005.
[15] K. Kataoka, N. Ohmura, M. Kouzu, Y. Simamura, M. Okubo, Emulsion polymerization of styrene in a continuous Taylor vortex flow reactor, Chem. Eng. Sci. 50 (1995) 1409–1416, https://doi.org/10.1016/0009-2509(94)00515-S.
[16] R.L.C. Giordano, R.C. Giordano, D.M.F. Prazeres, C.L. Cooney, Analysis of a Taylor-Poiseuille vortex flow reactor - II: reactor modeling and performance assessment using glucose-fructose isomerization as test reaction, Chem. Eng. Sci. 55 (2000) 3611–3626, https://doi.org/10.1016/S0009-2509(00)00052-X.
[17] B. Haut, H. Ben Amor, L. Coulon, A. Jacquet, V. Halloin, Hydrodynamics and mass transfer in a Couette-Taylor bioreactor for the culture of animal cells, Chem. Eng. Sci. 58 (2003) 777–784, https://doi.org/10.1016/S0009-2509(02)00607-3.
[18] J.S. Kim, D.H. Kim, B. Gu, D.Y. Kim, D.R. Yang, Simulation of Taylor-Couette reactor for particle classification using CFD, J. Cryst. Growth 373 (2013) 106–110, https://doi.org/10.1016/j.jcrysgro.2012.12.006.
[19] N. Shao, A. Gavriilidis, P. Angeli, Flow regimes for adiabatic gas-liquid flow in microchannels, Chem. Eng. Sci. 64 (2009) 2749–2761, https://doi.org/10.1016/j.ces.2009.01.067.
[20] M. Termühlen, M.M. Etmanski, I. Kryschewski, A.C. Kufner, G. Schembecker, K. Wohlgemuth, Continuous slug flow crystallization: impact of design and operating parameters on product quality, Chem. Eng. Res. Des. 170 (2021) 290–303, https://doi.org/10.1016/j.cherd.2021.04.006.
[21] Y. Takebayashi, K. Sue, S. Yoda, T. Furuya, K. Mae, Direct carbonylation of nitrobenzene to phenylisocyanate using gas-liquid slug flow in microchannel, Chem. Eng. J. 180 (2012) 250–254, https://doi.org/10.1016/j.cej.2011.11.031.
[22] A. Sauret, K. Somszor, E. Villermaux, E. Dressaire, Growth of clogs in parallel microchannels, Phys. Rev. Fluids 3 (2018) 1–18, https://doi.org/10.1103/PhysRevFluids.3.104301.
[23] E. Dressaire, A. Sauret, Clogging of microfluidic systems, Soft Matter 13 (2017) 37–48, https://doi.org/10.1039/C6SM01879C.
[24] D. Mowla, A. Naderi, Experimental study of drag reduction by a polymeric additive in slug two-phase flow of crude oil and air in horizontal pipes, Chem. Eng. Sci. 61 (2006) 1549–1554, https://doi.org/10.1016/j.ces.2005.09.006.

[25] K. Yamamoto, S. Ogata, Drag reduction of slug flows in microchannels by modifying the size of T-junctions, Int. J. Multiph. Flow 62 (2014) 67–72, https://doi.org/10.1016/j.ijmultiphaseflow.2014.02.011.
[26] J. yu Xu, Y. xiang Wu, H. Li, J. Guo, Y. Chang, Study of drag reduction by gas injection for power-law fluid flow in horizontal stratified and slug flow regimes, Chem. Eng. J. 147 (2009) 235–244, https://doi.org/10.1016/j.cej.2008.07.006.
[27] K.A. Triplett, S.M. Ghiaasiaan, S.I. Abdel-Khalik, D.L. Sadowski, Gas-liquid two-phase flow in microchannels part I: two-phase flow patterns, Int. J. Multiph. Flow. 25 (1999) 377–394, https://doi.org/10.1016/S0301-9322(98)00054-8.
[28] A.L. Dessimoz, P. Raspail, C. Berguerand, L. Kiwi-Minsker, Quantitative criteria to define flow patterns in micro-capillaries, Chem. Eng. J. 160 (2010) 882–890, https://doi.org/10.1016/j.cej.2010.01.011.
[29] Y. Yin, C. Zhu, R. Guo, T. Fu, Y. Ma, Gas-liquid two-phase flow in a square microchannel with chemical mass transfer: flow pattern, void fraction and frictional pressure drop, Int. J. Heat Mass Transf. 127 (2018) 484–496, https://doi.org/10.1016/j.ijheatmasstransfer.2018.07.113.
[30] C.Y. Yang, C.C. Shieh, Flow pattern of air-water and two-phase R-134a in small circular tubes, Int. J. Multiph. Flow. 27 (2001) 1163–1177, https://doi.org/10.1016/S0301-9322(00)00070-7.
[31] Y. Shiomi, H. Kutsuna, K. Akagawa, M. Ozawa, Two-phase flow in an annulus with a rotating inner cylinder (flow pattern in bubbly flow region), Nucl. Eng. Des. 141 (1993) 27–34, https://doi.org/10.1016/0029-5493(93)90089-R.
[32] R. Hubacz, S. Wroński, Horizontal Couette-Taylor flow in a two-phase gas-liquid system: flow patterns, Exp. Therm. Fluid Sci. 28 (2004) 457–466, https://doi.org/10.1016/j.expthermflusci.2003.07.004.
[33] R. Hubacz, Classification of flow regimes in gas-liquid horizontal Couette-Taylor flow using dimensionless criteria, J. Hydrodyn. 27 (2015) 773–781, https://doi.org/10.1016/S1001-6058(15)60539-X.
[34] S.J. Curran, R.A. Black, Oxygen transport and cell viability in an annular flow bioreactor: comparison of laminar couette and Taylor-vortex flow regimes, Biotechnol. Bioeng. 89 (2005) 766–774, https://doi.org/10.1002/bit.20361.
[35] C. Schäfer, A. Morozov, C. Wagner, Geometric scaling of elastic instabilities in the Taylor–Couette geometry: a theoretical, experimental and numerical study, J. Nonnewton. Fluid Mech. 259 (2018) 78–90, https://doi.org/10.1016/j.jnnfm.2018.06.002.
[36] J.G. Lim, S.H. Yoon, J. Hong, J.B. Choi, M.K. Kim, T.R. Lee, Continuous synthesis of nickel/cobalt/manganese hydroxide microparticles in Taylor–Couette reactors, J. Ind. Eng. Chem. 99 (2021) 388–395, https://doi.org/10.1016/j.jiec.2021.04.048.
[37] K. Kataoka, T. Mizusugi, H. Ueno, N. Ohmura, W.J. Yang, Heat Transfer and Fluid Flow in Rotating Machinery, Hemisphere publishing corporation, 1987, pp. 270–277.
[38] O. Levenspiel, The dispersion model. Chem. React. Eng., 3rd ed., John Wiley & Sons, Inc., 1999, pp. 293–320.
[39] R. Aris, The longitudinal diffusion coefficient in flow through a tube with stagnant pockets, Chem. Eng. Sci. 11 (1959) 194–198, https://doi.org/10.1016/0009-2509(59)80086-5.
[40] R.R. de Oliveira Silva, P.V.C. Calvo, C.A. Merfels, M.V.R. Lima, H.S. Santana, A. Converti, M.S.A. Palma, Synthesis of Lobeglitazone intermediates seeking for continuous drug production in flow capillary microreactor, J. Ind. Eng. Chem. 116 (2022) 239–249, https://doi.org/10.1016/j.jiec.2022.09.014.
[41] H. Zhou, X. Tang, Z. Wang, Y. Sun, X. Ling, Process performance and kinetics of the esterification of diketene to methyl acetoacetate in helical continuous-flow microreactors, Chem. Eng. Sci. 262 (2022), 117970, https://doi.org/10.1016/j.ces.2022.117970.
[42] W. Luo, F. Liu, Y. Guo, J. Qiu, J. Yan, S. Zhao, B. Bao, Continuous synthesis of dolutegravir sodium crystals using liquid-gas heterogeneous microreactor, Chin. Chem. Lett. (2022), https://doi.org/10.1016/j.cclet.2022.06.059.
[43] R.S. Abiev, C. Butler, E. Cid, B. Lalanne, A.M. Billet, Mass transfer characteristics and concentration field evolution for gas-liquid Taylor flow in milli channels, Chem. Eng. Sci. 207 (2019) 1331–1340, https://doi.org/10.1016/j.ces.2019.07.046.
[44] T. Makino, T. Kaise, K. Sasaki, N. Ohmura, K. Kataoka, Isolated mixing region in a taylor-vortex-flow reactor, Pdf 27 (2001) 566–573, https://doi.org/10.1252/kakoronbunshu.27.566.